

Phonon-Mediated versus Coulombic Backaction in Quantum Dot Circuits

D. Harbusch,¹ D. Taubert,¹ H. P. Tranitz,² W. Wegscheider,³ and S. Ludwig¹

¹*Center for NanoScience and Fakultät für Physik, Ludwig-Maximilians-Universität München, Geschwister-Scholl-Platz 1, D-80539 München, Germany*

²*Institut für Experimentelle Physik, Universität Regensburg, D-93040 Regensburg, Germany*

³*Laboratory for Solid State Physics, ETH Zürich, CH-8093 Zürich, Switzerland*

(Received 20 October 2009; published 10 May 2010)

Quantum point contacts (QPCs) are commonly employed to detect capacitively the charge state of coupled quantum dots (QDs). An indirect backaction of a biased QPC onto a double QD laterally defined in a GaAs/AlGaAs heterostructure is observed. Energy is emitted by nonequilibrium charge carriers in the leads of the biased QPC. Part of this energy is absorbed by the double QD where it causes charge fluctuations that can be observed under certain conditions in its stability diagram. By investigating the spectrum of the absorbed energy, we find that both acoustic phonons and Coulomb interaction can be involved in the backaction, depending on the geometry and coupling constants.

DOI: 10.1103/PhysRevLett.104.196801

PACS numbers: 73.21.La, 03.67.-a, 63.22.-m, 72.70.+m

Coupled quantum dots (QDs) are promising candidates for applications as qubits in solid state quantum information processing schemes [1]. One important criterion is the scalability of the qubit number. In a complex layout it will pose a great challenge to implement readout techniques that address single qubits without adding decoherence to the coupled QDs. Direct transport through an array of QDs is limited due to Coulomb blockade. In contrast, a single biased quantum point contact (QPC) in a separate circuit can act as charge detector for several QDs [2,3]. QPCs are straightforward to implement, yield sufficient sensitivity, and can be operated as wide bandwidth detectors [4,5]. The latter is desirable in quantum information processing where a rapid detection scheme is needed. The suitability of QPCs as fast detectors has been demonstrated in single-shot readout [6,7] and counting statistics experiments [8,9]. Increasing the bandwidth, however, requires a high signal-to-noise ratio which makes it necessary to operate the QPC at a relatively high bias voltage.

A biased QPC employed as a charge detector causes backaction. The fundamental Heisenberg backaction can be traced back to statistical charge fluctuations at the QPC capacitively coupled to QDs [10,11]. Shot noise only contributes to backaction if the QPC has resistive leads [10]. In addition to these direct Coulomb backaction mechanisms, the solid state environment provides possibilities for indirect backaction [12–15]. A biased QPC emits nonequilibrium charge carriers into its leads which then relax via electron-electron interaction, the emission of plasmons, or acoustic phonons [16]. Partial reabsorption of the emitted energy can result in charge fluctuations in (coupled) QDs, hence causing indirect backaction. Usually these fluctuations are too fast to be detected in measurements with limited bandwidth, but under certain conditions they can be observed in the stability diagram of coupled QDs [14]. In this Letter we present a systematic investigation of such backaction-induced charge fluctuations in a double QD.

We find that both acoustic phonons and Coulomb interaction can play an important role for the backaction in realistic devices.

Our device is based on a GaAs/AlGaAs heterostructure containing a two-dimensional electron system 90 nm beneath the surface. Charge carrier density and mobility are $n_e = 2.78 \times 10^{15} \text{ m}^{-2}$ and $\mu = 140 \text{ m}^2/\text{Vs}$. QDs and QPCs are electrostatically defined via metallic gates fabricated by e -beam lithography. The gate layout is shown in Fig. 1(a). The measurements are performed at an electron temperature of $T_{el} \lesssim 130 \text{ mK}$. Although the gate layout is designed for three QDs [17], here we define only a double QD (gates $d1$, $b1$ and α are grounded). Unless otherwise stated, only one of the implemented QPCs [black arrows in Fig. 1(a)] namely, QPC-I, is biased by applying a voltage V_{QPC} to contact IV. Since all other contacts are grounded and QPC-I is operated near pinch-off, the double QD is virtually unbiased. The dc current I_{QPC} flowing through QPC-I is measured with a bandwidth of only 10 Hz; I_{QPC} therefore probes the *average* charge configuration of the double QD. We obtain transconductance data $dI_{\text{QPC}}/dV_{\beta}$ by numerical differentiation of I_{QPC} . Having observed backaction in a wide range of charge configurations, here we focus on two electrons or less occupying the double QD. Solid lines in Fig. 1(b) sketch the expected charge stability diagram. Ground state configurations are denoted (N_B, N_C) , indicating that QD B (C) is occupied by N_B (N_C) electrons.

For the experiments presented here, it is essential to adjust the tunnel couplings of the double QD to be very asymmetric [14]. In a symmetric configuration, fundamental laws of thermodynamics prevent the observation of the backaction effects discussed here (see supplementary material [18]). In our case the right tunnel barrier $b2$ between QD C and lead III is almost closed, resulting in a tunneling rate of only $\Gamma_{b2} \approx 25 \text{ kHz}$. The interdot tunneling rate $\Gamma_{t2} \approx 0.7 \text{ GHz}$ between QD B and C , as well as Γ_{t1} be-

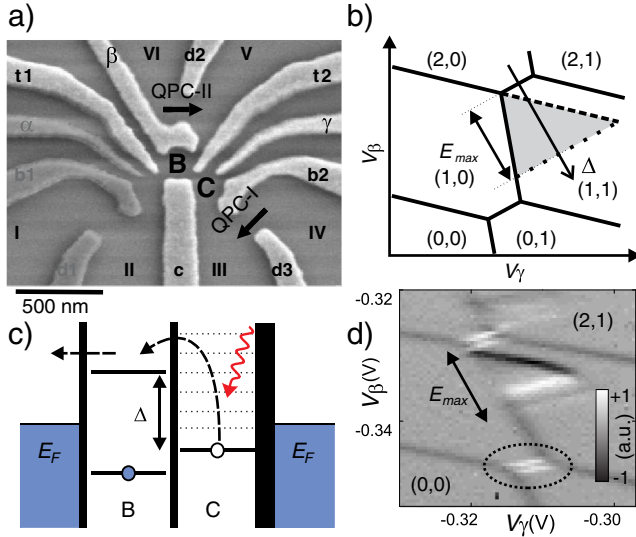


FIG. 1 (color online). (a) Scanning electron micrograph of an identical device. Metal gates (light gray) are negatively biased, darker gates are grounded. QDs (B , C), current paths (arrows), and Ohmic contacts (roman numbers) are indicated. (b) Sketch of a double QD charge stability diagram. Numbers in brackets indicate stable charge configurations (N_B , N_C). The gray triangle features backaction [compare (d)]. (c) Level diagram of the double QD. Dotted lines depict the electron excitation spectrum of QD C . (d) Measured transconductance dI_{QPC}/dV_β (gray scale) as a function of voltages applied to gates β and γ for $V_{QPC} = -1.6$ mV and $P_{QPC} = 0.64$ pW.

tween QD B and lead II are much higher. The measured charge stability diagram in Fig. 1(d) shows the transconductance dI_{QPC}/dV_β in gray scale as a function of the gate voltages V_β and V_γ . Two deviations from the usual ground state honeycomb pattern are observed. First, charge reconfiguration lines are split into double lines [circled in Fig. 1(d)]. In between these two white lines the dc current I_{QPC} versus V_β exhibits a plateau at a value reflecting an equal occupation of the configurations (1,0) and (0,1) [18]. This can be explained with rapid transitions between the symmetric and antisymmetric combinations of the two almost degenerate configurations [19]. The energy source driving these transitions is discussed below.

The second irregularity is a triangular-shaped region in the center of Fig. 1(d) described in more detail in Ref. [14]. Within the triangle, the charge in one of the QDs (here QD C) fluctuates. An electron from QD C tunnels to QD B and from there into lead II and vice versa: (1,1) \leftrightarrow (2,0) \leftrightarrow (1,0). As can be seen in Fig. 1(c), which shows the chemical potentials of the QDs and leads, these charge fluctuations require the absorption of energy. One of the border lines of the triangle in Fig. 1(d) is parallel to the charge reconfiguration lines (white double lines). Along this border line the energy difference Δ (asymmetry energy) between the ground state configurations (1,1) and (2,0) is thus constant [Figs. 1(b) and 1(c)]. With the charging energy of QD B (2.5 meV) the size of the triangle can

be converted into an energy E_{\max} [Figs. 1(b) and 1(d)]. We interpret E_{\max} as the maximum energy that QD C absorbs in a single process.

Figures 2(a) and 2(b) plot stability diagrams similar to that in Fig. 1(d) for two very different bias voltages V_{QPC} . The triangle size clearly grows with increasing bias indicating that QPC-I acts as the energy source. Figure 2(c) underlines this result. E_{\max} is plotted as a function of V_{QPC} and the dissipated power $P_{QPC} = I_{QPC}V_{QPC}$ with each data point corresponding to the size of one triangle. The curved surface fitted to the data is a guide to the eye. The gray plane in Fig. 2(c) is defined by $E_{\max} = eV_{QPC}$. This is the largest energy quantum the QPC can emit and the expected E_{\max} for backaction mediated by direct (first-order) Coulomb interaction, as compellingly suggested by previous data for the case of shot noise [20]. In our measurements, the open circles lie above this plane while the closed circles are below it. The apparently missing clear cutoff at $E_{\max} = eV_{QPC}$ [20] in Fig. 2(c) suggests that in our data direct backaction is unimportant. This has to be seen in the context of the very small conductance of our QPC, $G_{QPC} \ll 0.5G_0$, where $G_0 = 2e^2/h$. In this regime the direct backaction related to the shot noise of I_{QPC} or charge fluctuations at the QPC is expected to be strongly suppressed [11,18,21]. Especially, the deviations at large V_{QPC} , where we find $E_{\max} < eV_{QPC}$, imply indirect backaction with energy dissipated in the leads of the QPC. During the relaxation processes the energy spectrum is likely shifted towards lower energies before some of the resulting energy quanta are reabsorbed by the double QD.

E_{\max} strongly increases with P_{QPC} before it saturates at $P_{QPC} \approx 0.5$ pW [Fig. 2(c)]. The observation $E_{\max} < eV_{QPC}$ for very small P_{QPC} is another indication that the high energy end of the spectrum emitted by the QPC is suppressed in the absorption spectrum of the double QD. This

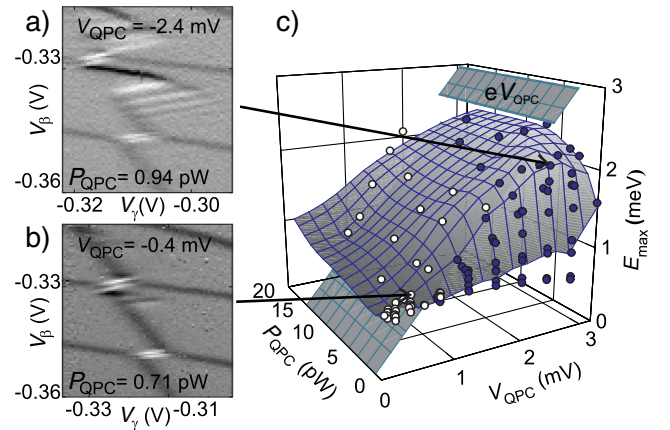


FIG. 2 (color online). (a),(b) Transconductance dI_{QPC}/dV_β (gray scale) as a function of V_β and V_γ . (c) Observed maximum of absorbed energy E_{\max} [compare Fig. 1(d)] as a function of P_{QPC} and V_{QPC} . Arrows show where (a) and (b) are located in this graph. See main text for details.

again suggests indirect backaction where multiple scattering processes in the leads of the QPC alter the original emission spectrum.

Our scenario of indirect backaction fails to explain $E_{\max} > eV_{\text{QPC}}$ in the regime of small V_{QPC} , and is in contrast to the observed lower bound of $E_{\max} \approx 0.6$ meV [open circles in Fig. 2(c)]. In the present experiment, this marks the limit of external nonthermal noise. It mainly consists of 50 Hz signals which stem from electronic instruments. Apparently, an asymmetrically coupled double QD can be employed as a sensitive noise detector.

The stability diagrams in Figs. 3(a) and 3(b) plot the current change δI_{QPC} at QPC-I [also compare Fig. 1(b)]. In Fig. 3(a) backaction is visible in the shape of a triangle of enhanced δI_{QPC} . Converting the gate voltage along the white line in Fig. 3(a) into the asymmetry energy Δ [defined in Fig. 1(c)] we plot cross sections through such triangles in Figs. 3(c)–3(e). In thermal equilibrium we expect the double QD to occupy its ground state configuration because of the low $T_{\text{el}} \approx 130$ mK. The y axis shows ΔI_{QPC} which is calculated from δI_{QPC} by subtracting the equilibrium value in configuration (1,1). To achieve comparability, the curves are scaled so that $\Delta I_{\text{QPC}} = 1$ in (1,0). The white line in Fig. 3(a) starts in configuration (2,0), crosses the area of (1,1) and ends in (0,1). The corresponding average values of ΔI_{QPC} measured at these configurations are indicated in Figs. 3(c)–3(e) as a shaded background. Figure 3(c) displays curves for different V_{QPC} in the high power limit of Fig. 2(c), while the power dependence is investigated in Fig. 3(d). All these curves follow approximately the behavior expected for thermal equilibrium (shaded background). Deviations are observed only at the backaction induced triangles located in the (1,1) area. Within these triangles the data display a general trend of an increasing ΔI_{QPC} with growing V_{QPC} and P_{QPC} . However, $\Delta I_{\text{QPC}} \approx 1$ represents an upper limit for all our measurements. Since the intermediate configuration (2,0) decays very fast into (1,0), ΔI_{QPC} indicates the average occupation number difference of the configurations (1,1) and (1,0). Wherever $\Delta I_{\text{QPC}} \approx 1$, the higher energy configuration (1,0) is strongly occupied. This can only be explained in terms of a nonequilibrium energy source driving the transitions.

All triangles induced by backaction of QPC-I can be divided into two regimes. For $0 < \Delta \leq 1.04$ meV [vertical dashed line in Figs. 3(c)–3(e)] we observe a featureless region where the current tends to saturate at $\Delta I_{\text{QPC}} \approx 1$. At $\Delta \approx 1.04$ meV the current sharply drops, and for $\Delta > 1.04$ meV, we find $\Delta I_{\text{QPC}} < 1$ even for large V_{QPC} and P_{QPC} . This region, however, features an additional substructure, best seen in Fig. 2(a), namely, lines of constant transconductance parallel to the charge reconfiguration lines. These lines correspond to constant detuning Δ between (1,1) and (2,0). They reveal the quantum mechanical excitation spectrum of QD C [compare Fig. 1(c)] [22]. Whenever an electron in QD C is lifted to an excited state

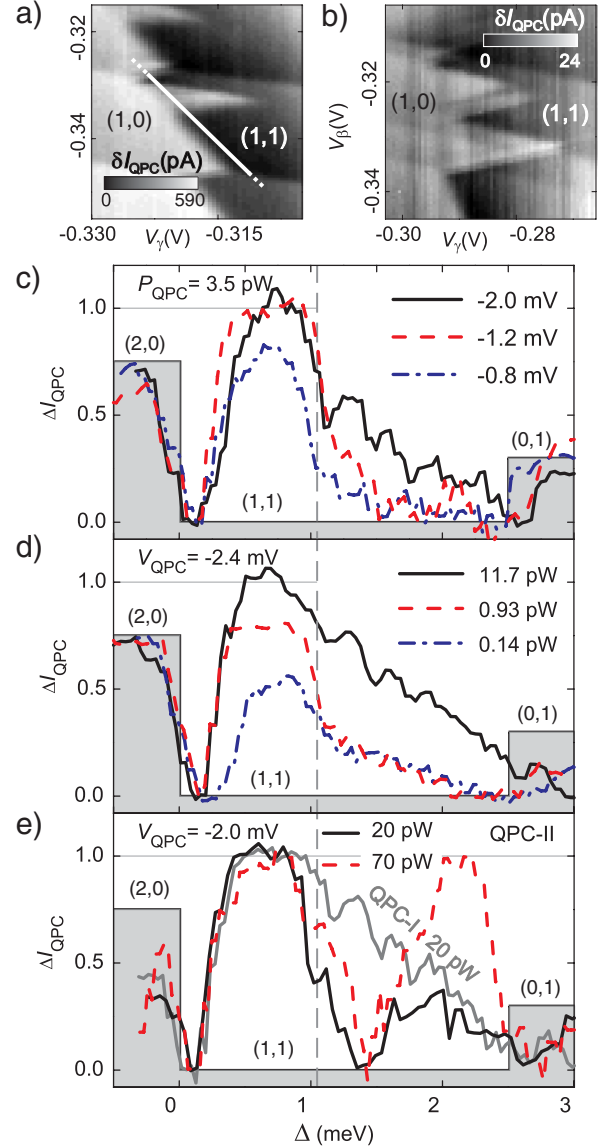


FIG. 3 (color online). (a),(b) δI_{QPC} (gray scale) as a function of V_{β} and V_{γ} . A plane fit is subtracted from I_{QPC} (resulting in δI_{QPC}) to correct for capacitances between gates and the QPC. In (a) only QPC-I is biased with $V_{\text{QPC}} = -0.8$ mV and $P_{\text{QPC}} = 2.5$ pW; for (b) the values are $V_{\text{QPC}} = -0.1$ mV and $P_{\text{QPC}} = 0.01$ pW. QPC-II is additionally biased in with $V_{\text{QPC}} = -2.0$ mV and $P_{\text{QPC}} = 72$ pW in (b). (c)–(e) Normalized current change ΔI_{QPC} versus asymmetry energy Δ [compare Fig. 1(c)] along the white line in (a). ΔI_{QPC} corresponding to configurations (2,0), (1,1) and (0,1) are highlighted in gray.

(1,1)*, that is in resonance with the ground state of (2,0), tunneling between the two QDs is enhanced. This leads to the observed alternating occupation probability as a function of Δ . Although we expect additional excited states of QD C, we do not observe them at $\Delta < 1.04$ meV.

We explain the sharp current drop at $\Delta \approx 1.04$ meV as follows. In Ref. [23] phonon-mediated interaction in mesoscopic circuits has been demonstrated. Backscattering of an electron defines an upper limit $E_{\max}^{\text{ph}} \approx 2\hbar k_{\text{F}} v_s$

for the energy that can be transferred to an acoustic phonon [23]. With our Fermi energy of $E_F \approx 10$ meV and the maximum sound velocity $v_s \approx 6000$ m/s from Ref. [23], we find $E_{\max}^{\text{ph}} \approx 1.04$ meV. Just at this asymmetry $\Delta = E_{\max}^{\text{ph}}$ the current drops sharply [Figs. 3(c)–3(e)]. We conclude that for $\Delta \approx 1.04$ meV the backaction is mainly caused by phonons emitted in the leads of the biased QPC and reabsorbed by a QD. Absorption of multiple phonons could account for backaction observed for $\Delta > 1.04$ meV. However, the existence of two different interaction mechanisms seems more likely, because of the observation of the excitation spectrum of QD *C* only for $\Delta > 1.04$ meV.

For the data shown in Figs. 3(b) and 3(e), QPC-II is strongly biased and used as the energy emitter (while the weakly biased QPC-I is still the detector). Figure 3(e) displays an additional measurement for QPC-I (gray solid line) as the emitter. When QPC-II is strongly driven, ΔI_{QPC} drops all the way to zero near $\Delta \approx 1.04$ meV. Then, for $\Delta > 1.04$ meV, a second triangle of charge fluctuations appears, as can be best observed in Fig. 3(b). Both triangles have no substructure. This is in direct contrast to the results obtained with QPC-I as the emitter, where we observe a characteristic substructure for $\Delta > 1.04$ meV [parallel lines in Fig. 2(a)], namely, the excitation spectrum of QD *C*.

An important difference between the two QPCs is, that the capacitive coupling between the double QD and QPC-I is roughly twice as large compared to QPC-II. Experimentally we find that the excitation spectrum of QD *C* can only be resolved if QPC-I is the emitter, where the capacitive coupling between QD *C* and the energy emitting QPC (and its leads) is strong. These results imply that Coulomb interaction is the dominant backaction mechanism for $\Delta > 1.04$ meV. At the same time, the observed backaction must be indirect [as discussed above, see Fig. 2(c)]. We suggest a mechanism in which nonequilibrium charge carriers are emitted by QPC-I. Next, excited carriers in lead III exchange energy with QD *C* via Coulomb interaction. This scenario explains the remaining backaction for $\Delta > 1.04$ meV when QPC-I is the emitter.

The position of the second (lower) triangle in Fig. 3(b) indicates transitions involving the configurations $(1, 1) \leftrightarrow (0, 1) \leftrightarrow (1, 0)$ compared to $(1, 1) \leftrightarrow (2, 0) \leftrightarrow (1, 0)$ for the upper triangle. Here the electron in QD *B* tunnels to lead II after absorbing energy, then the electron in QD *C* relaxes to QD *B* (and emits energy). To first order, the transition $(1, 1) \rightarrow (0, 1)$ cannot be driven by phonons ($(1, 1) \rightarrow (2, 0)$ for the upper triangle) whenever the energy difference between these two configurations exceeds $E_{\max}^{\text{ph}} \approx 1.04$ meV. In fact, the size of both triangles in Fig. 3(b) [and the width of both local maxima in Fig. 3(e)] are identical and equal to E_{\max}^{ph} . This result strongly points to phonon-mediated backaction for both triangles. Note that

for $P_{\text{QPC}} > 15$ pW, the second phonon-mediated triangle is also weakly visible with QPC-I as the emitter [18]. The apparent difference in interaction strength can be partly explained by the anisotropic coupling tensors between electrons and phonons and the sample geometry.

In conclusion, we demonstrate a method to directly measure backaction of a biased QPC on a double QD causing charge fluctuations. Backaction spectroscopy allows us to identify phonon-induced backaction as well as features most likely caused by Coulomb interaction. The observed backaction is indirect in nature, distinguishing it from the direct Coulomb interaction between charge fluctuations at the QPC and the electrons confined in QDs. Comparing two different QPCs reveals a strong dependence of the backaction on geometry. Our results will help to develop detectors with reduced backaction.

We thank J. P. Kotthaus, G. J. Schinner, T. Ihn, and D. M. Eigler for fruitful discussions. Financial support by the German Science Foundation via SFB 631 and SFB 689, the German Israel program DIP, the German Excellence Initiative via the “Nanosystems Initiative Munich (NIM)”, and LMUinnovativ (FuNS) is gratefully acknowledged.

-
- [1] D. Loss and D. P. DiVincenzo, *Phys. Rev. A* **57**, 120 (1998).
 - [2] M. Field *et al.*, *Phys. Rev. Lett.* **70**, 1311 (1993).
 - [3] J. M. Elzerman *et al.*, *Phys. Rev. B* **67**, 161308(R) (2003).
 - [4] D. J. Reilly, C. M. Marcus, M. P. Hanson, and A. C. Gossard, *Appl. Phys. Lett.* **91**, 162101 (2007).
 - [5] M. C. Cassidy *et al.*, *Appl. Phys. Lett.* **91**, 222104 (2007).
 - [6] J. Elzerman *et al.*, *Nature (London)* **430**, 431 (2004).
 - [7] C. Barthel *et al.*, *Phys. Rev. Lett.* **103**, 160503 (2009).
 - [8] S. Gustavsson *et al.*, *Phys. Rev. Lett.* **96**, 076605 (2006).
 - [9] C. Fricke, F. Hohls, W. Wegscheider, and R. J. Haug, *Phys. Rev. B* **76**, 155307 (2007).
 - [10] R. Aguado and L. P. Kouwenhoven, *Phys. Rev. Lett.* **84**, 1986 (2000).
 - [11] C. E. Young and A. A. Clerk, *Phys. Rev. Lett.* **104**, 186803 (2010).
 - [12] V. S. Khrapai *et al.*, *Phys. Rev. Lett.* **97**, 176803 (2006).
 - [13] V. S. Khrapai *et al.*, *Phys. Rev. Lett.* **99**, 096803 (2007).
 - [14] D. Taubert *et al.*, *Phys. Rev. Lett.* **100**, 176805 (2008).
 - [15] U. Gasser *et al.*, *Phys. Rev. B* **79**, 035303 (2009).
 - [16] B. Ridley, *Rep. Prog. Phys.* **54**, 169 (1991).
 - [17] D. Schröer *et al.*, *Phys. Rev. B* **76**, 075306 (2007).
 - [18] See supplementary material at <http://link.aps.org/supplemental/10.1103/PhysRevLett.104.196801>.
 - [19] A. W. Rushforth *et al.*, *Phys. Rev. B* **69**, 113309 (2004).
 - [20] S. Gustavsson *et al.*, *Phys. Rev. Lett.* **99**, 206804 (2007).
 - [21] M. Reznikov, M. Heiblum, H. Shtrikman, and D. Mahalu, *Phys. Rev. Lett.* **75**, 3340 (1995).
 - [22] The spacing of the energy levels decreases monotonically from 310 μeV to 230 μeV with increasing Δ , suggesting a softer confinement potential as in the harmonic case.
 - [23] G. J. Schinner *et al.*, *Phys. Rev. Lett.* **102**, 186801 (2009).